

# Gamma-ray emission from individual classical novae

Jordi Gómez-Gomar,<sup>1</sup> Margarita Hernanz,<sup>1</sup> Jordi José<sup>1,2</sup> and Jordi Isern<sup>1</sup>

<sup>1</sup> *Institut d'Estudis Espacials de Catalunya, CSIC Research Unit, Edifici Nexus-104, C/Gran Capità, 2-4, E-08034 Barcelona, SPAIN*

<sup>2</sup> *Departament de Física i Enginyeria Nuclear (UPC), Avda. Víctor Balaguer, s/n, E-08800 Vilanova i la Geltrú (Barcelona), SPAIN*

15 October 2018

## ABSTRACT

Classical novae are important producers of radioactive nuclei, such as  ${}^7\text{Be}$ ,  ${}^{13}\text{N}$ ,  ${}^{18}\text{F}$ ,  ${}^{22}\text{Na}$  and  ${}^{26}\text{Al}$ . The disintegration of these nuclei produces positrons (except for  ${}^7\text{Be}$ ) that through annihilation with electrons produce photons of energies 511 keV and below. Furthermore,  ${}^7\text{Be}$  and  ${}^{22}\text{Na}$  decay producing photons with energies of 478 keV and 1275 keV, respectively, well in the  $\gamma$ -ray domain. Therefore, novae are potential sources of  $\gamma$ -ray emission. We have developed two codes in order to analyze carefully the  $\gamma$ -ray emission of individual classical novae: a hydrodynamical one, which follows both the accretion and the explosion stages, and a Monte-Carlo one, able to treat both the production and the transfer of  $\gamma$ -ray photons. Both codes have been coupled in order to simulate realistic explosions. The properties of  $\gamma$ -ray spectra and  $\gamma$ -ray light curves (for the continuum and for the lines at 511, 478 and 1275 keV) have been analyzed, with a special emphasis on the difference between carbon-oxygen and oxygen-neon novae. Predictions of detectability of individual novae by the future SPI spectrometer on board the INTEGRAL satellite are made. Concerning  ${}^{26}\text{Al}$ , its decay produces photons of 1809 keV but it occurs on a timescale much longer than the typical time interval between nova outbursts in the Galaxy, making it undetectable in individual novae. The accumulated emission of  ${}^{26}\text{Al}$  from many Galactic novae has not been modeled in this paper.

**Key words:** gamma-rays: general - novae, cataclysmic variables - nucleosynthesis - stars: abundances - white dwarfs

## 1 INTRODUCTION

Thermonuclear runaways on accreting white dwarfs are at the origin of nova explosions. Some unstable proton-rich nuclei, such as  ${}^{13}\text{N}$ ,  ${}^{14}\text{O}$ ,  ${}^{15}\text{O}$ ,  ${}^{17}\text{F}$  and  ${}^{18}\text{F}$ , are produced during hydrogen-burning. These nuclei are  $\beta^+$ -unstable and therefore decay through the emission of positrons. This has two important consequences. First of all, the decay times of  ${}^{14}\text{O}$  ( $\tau=102\text{s}$ ),  ${}^{15}\text{O}$  ( $\tau=176\text{s}$ ) and  ${}^{17}\text{F}$  ( $\tau=93\text{s}$ ) are such that these nuclei can be transported by convection to the outer layers of the envelope (during the runaway) before decaying; their subsequent decay in these outer shells of the envelope is largely responsible for the expansion and of the large increase in luminosity of the nova. Second, the positrons emitted by all those nuclei annihilate with electrons leading to the emission of photons with energy equal or below 511 keV.  ${}^{13}\text{N}$  ( $\tau=862\text{s}$ ) and  ${}^{18}\text{F}$  ( $\tau=158\text{min}$ ) are the most important contributors to  $\gamma$ -ray emission, since their decay timescales are larger and they decay when the envelope is transparent enough. Other radioactive elements are synthesized during nova explosions: carbon-oxygen (CO) novae are important producers of  ${}^7\text{Be}$  ( $\tau=77\text{days}$ ) (see Hernanz et al. 1996), which emits a photon of 478 keV when it

decays through an electron capture, whereas oxygen-neon-magnesium novae (ONeMg) produce  ${}^{22}\text{Na}$  ( $\tau=3.75\text{yr}$ ) and  ${}^{26}\text{Al}$  ( $\tau=1.04\times 10^6\text{yr}$ ), which decay emitting a positron and a photon of 1275 and 1809 keV, respectively.

Some previous works have pointed out the potential importance of classical novae as  $\gamma$ -ray emitters (Clayton 1981, Clayton & Hoyle 1974, Leising & Clayton 1987). Concerning the nucleosynthesis of radioactive nuclei in novae, it has been analyzed by means of parametrized studies (Weiss & Truran 1990, Nofar, Shaviv & Starrfield 1991), and by complete hydrodynamic simulations (see Politano et al. 1995 and Pralnik & Kovetz 1997, for recent works concerning ONeMg and CO novae, respectively, and also José & Hernanz 1997). But there is a lack of detailed studies of the  $\gamma$ -ray output of novae and its relation with the production of radioactive nuclei. Only the use of realistic profiles of velocities, densities and chemical abundances, necessary to know the production and transfer of  $\gamma$ -rays during nova explosions, will provide the correct  $\gamma$ -ray spectra of classical novae (Hernanz et al. 1997a and b).

From the observational point of view, two types of observations have to be distinguished: individual and cumulative. The emission of short and medium-lived radioactive

arXiv:astro-ph/9711322v2 1 Apr 1998

nuclei (478, 511 and 1275 keV lines and continuum) can be detected in individual novae, provided they are close enough. The emission of very long-lived  $^{26}\text{Al}$  nuclei can contribute to the diffuse emission in the Galaxy, but can not be detected in particular novae. The emission of the medium-lived nuclei ( $^7\text{Be}$  and  $^{22}\text{Na}$  at 478 and 1275 keV) can also be accumulated from different novae, as their lifetimes are longer than the typical time interval between two consecutive nova explosions in the Galaxy. Up to now, no positive detection of novae in  $\gamma$ -rays has been produced, neither for particular novae in the 478 or 1275 keV lines (Harris, Leising & Share 1991, Iyudin et al. 1995), nor for the cumulative emission of novae at the Galactic center in these same lines (Leising et al. 1988, Harris et al. 1991 and 1996).

We will concentrate in this paper on the  $\gamma$ -ray emission from individual novae, by means of hydrodynamical simulations which include both the accretion and explosion stages, with complete nucleosynthesis, and a Monte-Carlo technique to follow the production and transfer of  $\gamma$ -ray photons. The analysis of the cumulative emission from novae in the Galaxy is currently under way. The nova models are presented in section 2, with special emphasis on the synthesis of radioactive nuclei and their density and velocity profiles. In section 3 we describe the Monte-Carlo simulation technique and in section 4 its results, in the form of  $\gamma$ -ray spectra and light curves for the continuum and the main lines of interest. Finally, our discussion and conclusions follow.

## 2 NUCLEOSYNTHESIS OF RADIOACTIVE NUCLEI

The accretion and explosion stages have been followed by means of an implicit hydrodynamic code, which includes a complete nuclear reaction network; one hundred nuclei, ranging from  $^1\text{H}$  to  $^{40}\text{Ca}$ , linked through 370 nuclear reactions, have been included (see José 1996 and José & Hernanz 1997a and b, for details). A time-dependent formalism for convective transport has been included whenever the characteristic convective timescale becomes larger than the integration time step (Wood 1974). Partial mixing between adjacent shells is treated as a diffusion process (Priyalnik, Shara & Shaviv 1979). CO as well as ONeMg novae have been computed, with an accretion rate of  $2 \times 10^{-10} M_{\odot} \text{yr}^{-1}$  (other values for the accretion rate have also been considered, but they do not introduce noticeable changes in the properties of the radioactive nuclei synthesized). The initial composition of nova envelopes is far from being understood, but some enrichment with material from the white dwarf core is needed in order to explain both the explosion mechanism itself and some of the observed abundances in novae. Thus, as the real mechanism of enhancement is not clear at present, a compromise solution consisting of a parametrized mixture between the outermost shells of the underlying core and the solar-like accreted matter is adopted. We have assumed a 50% degree of mixing, although other possibilities have also been analyzed. For the CO novae, the adopted composition of the underlying core consists of a 50%-50% mixture of  $^{12}\text{C}$  and of  $^{16}\text{O}$ , whereas for ONeMg novae (where the initial composition is more crucial for the synthesis of the radioactive nucleus  $^{22}\text{Na}$ ) we have adopted a detailed outer core initial composition from Ritossa, García-Berro

& Iben (1996) (indicating that these white dwarfs are almost devoid of magnesium, which makes it more correct to call them oxygen-neon (ONe) white dwarfs). The exact initial composition is an important issue, since the presence of  $^{20}\text{Ne}$  and its amount, as well as that of magnesium, is crucial for the final amount of the radioactive nuclei  $^{22}\text{Na}$  and  $^{26}\text{Al}$ . In particular, the new initial abundances we are using favor a lower  $^{22}\text{Na}$  and  $^{26}\text{Al}$  production than the ones commonly adopted, based on old nucleosynthesis calculations by Arnett & Truran (1969) (José, Hernanz & Coc 1997, José & Hernanz 1997a and b). Recent observations of individual novae with the COMPTEL instrument on board the COMPTELON Gamma-Ray Observatory (CGRO) have not detected the 1275 keV emission in any of the observed novae. Only upper limits to the flux, which translate into upper limits to the  $^{22}\text{Na}$  ejected mass, were obtained (Iyudin et al. 1995). COMPTEL observations have also provided detailed maps of the Galactic 1809 keV emission, corresponding to  $^{26}\text{Al}$  decay (Diehl et al. 1995). The main features of these maps seem to indicate that this emission is rather correlated with a young population, thus discarding novae as the main contributors to it (see Prantzos & Diehl 1996 for a recent review). Our low  $^{22}\text{Na}$  and  $^{26}\text{Al}$  yields are consistent with both observational results.

The production of radioactive nuclei, as well as some other relevant properties, of some selected CO and ONe novae are displayed in Table 1 (see José and Hernanz 1997a and b for more details). Models A1 and A2 correspond to ONe novae with masses  $1.15 M_{\odot}$  and  $1.25 M_{\odot}$ , respectively, whereas models B1 and B2 correspond to CO novae, with masses 0.8 and  $1.15 M_{\odot}$ , respectively. Models A1, A2 and B2 share some general properties: they have similar ejected masses ( $\sim 10^{-5} M_{\odot}$ ) and similar kinetic energies ( $\sim 3 \times 10^{16} \text{erg.g}^{-1}$ ), with typical average velocities between 2000 and  $3000 \text{km.s}^{-1}$ . Concerning model B1, its lower initial mass leads to a higher mass of the accreted envelope and thus to a higher ejected mass but with a lower mean velocity ( $\sim 1000 \text{km.s}^{-1}$ ), which translates into a lower kinetic energy. This makes this model more opaque to the  $\gamma$ -rays, as will be shown below. Concerning the synthesis of radioactive nuclei, the most important result is that  $^7\text{Be}$  is mainly produced in CO novae whereas  $^{22}\text{Na}$  is only produced in ONe novae. This result is a consequence of the different initial compositions of CO and ONe novae, as discussed above. The complete profiles of density, velocity and chemical composition obtained with the hydrodynamical code, taken when the unaccelerated expansion begins, have been used as inputs for the calculations performed with the Monte-Carlo code developed to obtain the gamma-ray emission of those classical novae.

## 3 GAMMA-RAY PRODUCTION AND PROPAGATION: MONTE-CARLO SIMULATION

In order to simulate the evolution of the  $\gamma$ -ray spectra of the different models of novae considered, we have developed a  $\gamma$ -ray transfer code on the basis of the method described by Pozdnyakov, Sobol & Sunyaev (1983) and Ambwani & Sutherland (1988). This code has been successfully applied to the study of the spectra of type Ia supernovae (Gómez-Gomar, Isern & Jean 1997). It is based on the Monte-Carlo

**Table 1.** Main properties of the ejecta one hour after peak temperature.

Model	$M_{\text{wd}}$	$M_{\text{ejec}}$	$\langle E_k \rangle$	${}^7\text{Be}$	${}^{13}\text{N}$	${}^{18}\text{F}$	${}^{22}\text{Na}$
A1	1.15	$1.8 \cdot 10^{-5}$	$3.1 \cdot 10^{16}$	$\sim 0$	$5.5 \cdot 10^{-9}$	$7.1 \cdot 10^{-8}$	$9.8 \cdot 10^{-10}$
A2	1.25	$1.6 \cdot 10^{-5}$	$3.3 \cdot 10^{16}$	$1.2 \cdot 10^{-11}$	$2.9 \cdot 10^{-8}$	$6.7 \cdot 10^{-8}$	$1.6 \cdot 10^{-9}$
B1	0.8	$6.3 \cdot 10^{-5}$	$8 \cdot 10^{15}$	$7.8 \cdot 10^{-11}$	$1.6 \cdot 10^{-7}$	$1.7 \cdot 10^{-7}$	$\sim 0$
B2	1.15	$1.4 \cdot 10^{-5}$	$3.2 \cdot 10^{16}$	$1.1 \cdot 10^{-10}$	$1.3 \cdot 10^{-8}$	$3.6 \cdot 10^{-8}$	$\sim 0$

$M_{\text{wd}}$ , total ejected mass ( $M_{\text{ejec}}$ ) and ejected mass of each isotope are in  $M_{\odot}$ , and the average kinetic energy  $\langle E_k \rangle$  is in  $\text{erg g}^{-1}$ . Models A1 and A2 correspond to ONe novae, whereas B1 and B2 are CO ones.

technique, which allows to treat the comptonization of high energy photons without approximations. In the code, the radioactive decays of  ${}^7\text{Be}$ ,  ${}^{13}\text{N}$ ,  ${}^{18}\text{F}$  and  ${}^{22}\text{Na}$  are included to generate the initial photons. A comment must be made regarding  ${}^7\text{Be}$ . This nucleus decays via the capture of an electron of the K-shell. This implies that at high temperatures its decay time in the laboratory could change because of ionization. However, as the lifetime of this nucleus is quite long we assume that for most of the time the temperature of the envelope is low enough to avoid complete ionization and the decay time is always taken to be equal to the laboratory time.

Once photons are generated according to the relative isotopic abundances and rates of disintegration of the above mentioned radioactive nuclei, their trip across the expanding ejecta is simulated by taking into account the three different interactions which affect their propagation, i.e. Compton scattering, photoelectric absorption and production of  $e^-e^+$  pairs. The cross sections for all these interactions is computed taking into account the precise composition of the ejecta. In the case of Compton scattering the cross section adopted is the usual Klein-Nishina expression, while absorption and pair production cross sections are taken from the compilation of experimentally evaluated data maintained by the Brookhaven National Laboratory. In the code the effects of the expansion velocity are included an thus realistic line profiles are obtained. Besides direct emission by radioactive decay, photons are also emitted by positron annihilation.

The treatment of positron annihilation has required particular attention, since during some phases of the nova evolution this is the dominant emission mechanism, being  ${}^{13}\text{N}$ ,  ${}^{18}\text{F}$  and  ${}^{22}\text{Na}$  the main contributors. When a positron is emitted, either it escapes without interaction with the ejecta or it annihilates. We have considered that in a nova envelope positrons thermalize before annihilating. This approximation is wrong in less than 1% of the cases in an electronic plasma (Leising & Clayton 1987). Concerning a neutral envelope, the excitation cross section dominates any other interaction above energies of  $\sim 100$  eV (Bussard, Ramaty & Drachman 1979) and thus positrons lose energy until they reach this extremely low value. To reproduce this braking effect in the simulations, positrons propagate until they cross an equivalent column mass density of  $0.2 \text{ g cm}^{-2}$  (measured in straight line) (Chan & Lingenfelter 1993). This is the mean range expected for a 0.6 MeV positron braked down to energies  $\sim 100$  eV through elastic collisions with the surrounding medium, and neglecting the effects of the magnetic field on its propagation. When a positron is thermalized, it covers a negligible distance and then annihilates. For temperatures and densities of a nova envelope the positrons form positronium in  $\sim 90$  % of annihilations (Leising & Clay-

ton 1987) while in the remaining 10 % of cases they annihilate directly. 25% of times positronium is formed in singlet state, which leads to the emission of two 511 keV photons, while 75% of times it is formed in triplet state, leading to a three photon annihilation. The continuum spectrum of photons produced by triplet annihilations is obtained from the results of Ore & Powell (1949). To summarize, once a positron is produced we follow its trip until it escapes or covers the average energy loss distance. In the latter case it produces positronium 90% of times leading to triplet to singlet annihilations in the proportion 3:1, while in 10 % of the cases it annihilates directly.

## 4 GAMMA-RAY SPECTRA AND LIGHT CURVES

The  $\gamma$ -ray signatures of CO and ONe novae are very different. In the CO case, an important production of  ${}^7\text{Be}$  ensues (Hernanz et al. 1996), leading to line emission at 478 keV. There is also line emission at 511 keV, related to  $e^-e^+$  annihilation, and a continuum related to comptonized 511 keV emission and positronium decay (see below for details). On the other hand, ONe novae are  ${}^{22}\text{Na}$  producers, leading to line emission at 1275 keV (plus the 511 keV and below emission similar to the one of the CO cases).

In figures 1, 2, 3 and 4 the spectral evolution of models A1, A2, B1 and B2, representing the emission expected for these novae at a distance of 1 kpc, is shown. These sequences correspond to the early stages of the nova outburst up to 2 days after peak temperature. In all cases a continuum component, basically below 511 keV, as well as some lines (478 keV, 511 keV and 1275 keV) appear. The relative intensity of the continuum and the lines, the particular lines appearing and the temporal evolution of the spectra depend on the model considered. In what follows we will discuss in detail the properties of the continuum and the lines.

### 4.1 Continuum

In all models a strong continuum dominates the spectrum during the early epochs of the expansion, when the ejecta is optically thick. It is produced both by the comptonization of photons emitted in the 511 keV line and by the photons directly emitted in the continuum by positronium annihilation. In order to display the evolution of the continuum in all models, we have computed the  $\gamma$ -ray light curves for the emission in a band ranging from 170 keV to 470 keV (see fig. 5). This band contains most of the continuum and no appreciable contribution of the 478 and 511 keV lines. Furthermore, it avoids energies where the instrumental background

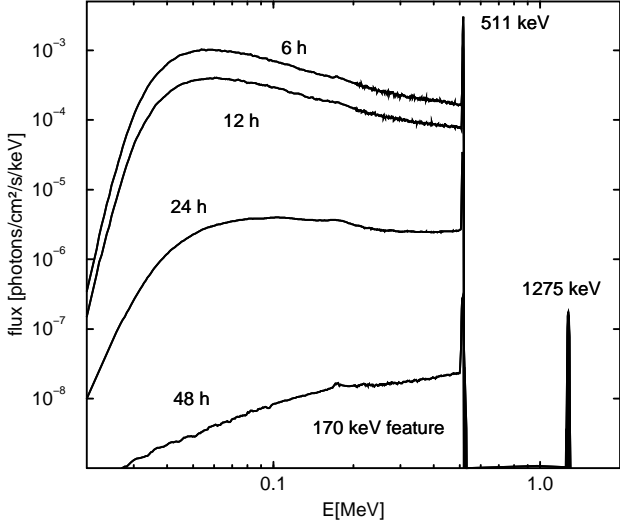


**Figure 1.** Evolution of the  $\gamma$ -ray spectrum of model A1 ( $1.15 M_{\odot}$ , ONe nova;  $d=1$  kpc). Spectra correspond to 6, 12, 24 and 48 hours after peak temperature. Notice that the 1275 keV line has not yet reached its maximum flux at  $t=48$  h (see Table 3 and Figure 6).

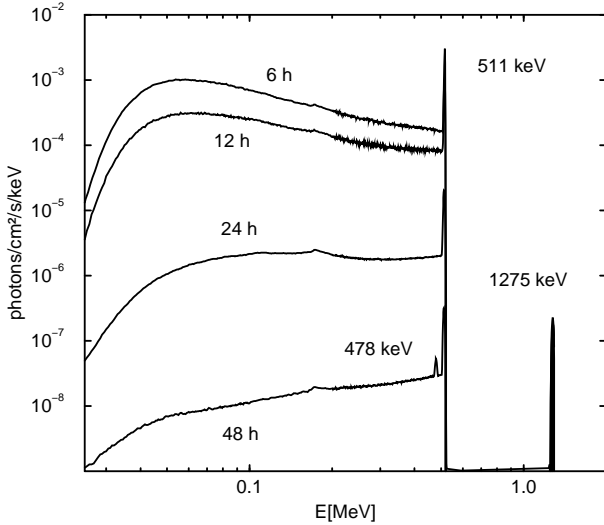


**Figure 2.** Evolution of the  $\gamma$ -ray spectrum of model A2 ( $1.25 M_{\odot}$ , ONe nova;  $d=1$  kpc). Spectra correspond to 6, 12, 24 and 48 hours after peak temperature.

for the SPI spectrometer on board the future INTEGRAL satellite will be higher (Jean 1995). The duration of this period is determined by the mass of the ejecta and its expansion rate, being longer for more massive envelopes. As shown in figure 5, a reduction of the flux by a factor of 100 occurs at around day 1. In this phase, the main source of  $\gamma$ -ray photons is the annihilation of positrons coming from the decay of  $^{13}\text{N}$  and  $^{18}\text{F}$ . In all cases the continuum displays a cutoff at low energies (see figs. 1 to 4). During the first hours, the cutoff is caused by photoelectric absorption, which has larger cross sections than Compton scattering at low ener-

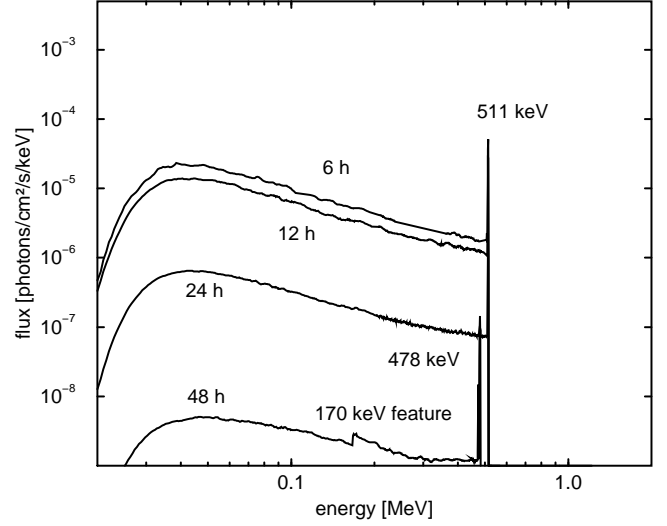


**Figure 3.** Evolution of the  $\gamma$ -ray spectrum of model B1 ( $0.8 M_{\odot}$ , CO nova;  $d=1$  kpc). Spectra correspond to 6, 12, 24 and 48 hours after peak temperature.

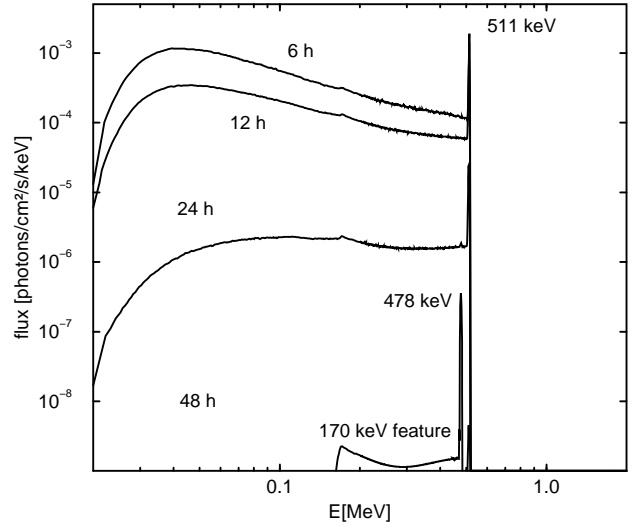


**Figure 4.** Evolution of the  $\gamma$ -ray spectrum of model B2 ( $1.15 M_{\odot}$ , CO nova;  $d=1$  kpc). Spectra correspond to 6, 12, 24 and 48 hours after peak temperature.

gies and acts as a sink of comptonized photons. Because of the strong effect of the composition on the cross section of photoelectric absorption, the cutoff is located at higher energies for the ONe rich envelopes ( $\sim 30$  keV to be compared to  $\sim 20$  keV for CO models). As the ejecta expands, the optical thickness of the envelope decreases and comptonization becomes unable to “pump” photons to low energies, leading to the shift of the cutoff towards higher energies and to smoother slopes. When the ejecta becomes transparent, the contribution of comptonization to the continuum completely disappears and the continuum corresponds exclusively to the photons coming from positronium annihilation, which displays its intrinsic emission spectrum (Ore

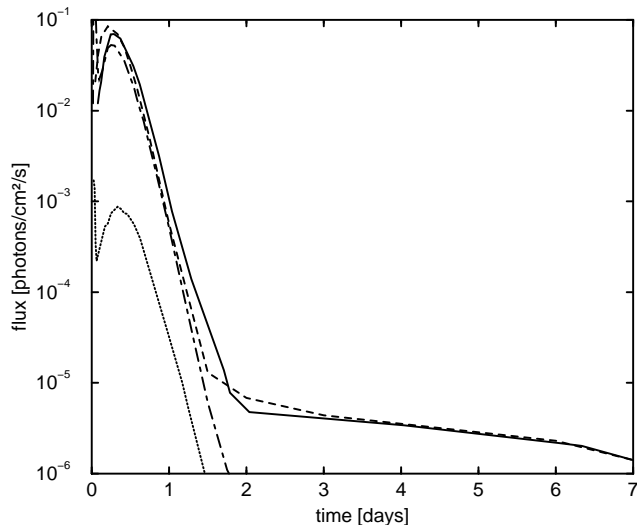


**Figure 5.** Evolution of the  $\gamma$ -ray emission in the band 170 keV–470 keV ( $d=1$  kpc) for the different models. Solid line corresponds to model A1 ( $1.15 M_{\odot}$ , ONe nova), dashed line to model A2 ( $1.25 M_{\odot}$ , ONe), dotted line to model B1 ( $0.8 M_{\odot}$ , CO), and dot-dashed line to model B2 ( $1.15 M_{\odot}$ , CO).

& Powell 1949). In the transition from an optically thick to an optically thin envelope, a feature appears at 170 keV (the energy of a backscattered 511 keV photon) which is related to the fact that very few photons are scattered more than once, leading to a steep decrease of the continuum intensity at this energy (see figs. 1 to 4). In the case of CO novae (models B1 and B2), after the decay of  $^{13}\text{N}$  and  $^{18}\text{F}$  no relevant  $e^+$  emitters are left and the continuum practically disappears (flux  $F \leq 10^{-6}$  photons/s/cm $^2$ ) between days 1 and 2. However, for ONe novae (models A1 and A2)  $^{22}\text{Na}$  is a secondary source of  $e^+$ , with a longer lifetime than  $^{13}\text{N}$  and  $^{18}\text{F}$ . It emits a  $e^+$  in 90 % of its decays. For these models, the continuum would in principle decline with the decay time of  $^{22}\text{Na}$  (3.75 years); however, when the ejecta is so transparent that even the positrons generated by the decay of  $^{22}\text{Na}$  can escape without interacting with matter, the continuum disappears. This happens at  $t \sim 7.5$  days for models A1 and A2 (see fig. 5).

The maximum for the emission in the continuum coincides with that for the 511 keV line in all cases, as we will see below (fig. 8). It appears around 5–6 hours after peak temperature. This maximum is mainly associated with the decay of  $^{18}\text{F}$  ( $\tau=2.6$  hours). However, in models B1 and B2 a previous and stronger maximum appears around one hour after peak temperature, caused by the emission of the short-lived  $^{13}\text{N}$ . This maximum is related to the high abundance of  $^{13}\text{N}$  in the outer layers of these models. In Table 2 the positions and intensities of these maxima, as well as the moment when the continuum intensity falls below  $10^{-6}$  photons/s/cm $^2$  ( $t_{\text{off}}$ ) are summarized.

Although the continuum duration is very short as compared to the nominal observation times of INTEGRAL’s SPI instrument, its large intensity during this short period makes it interesting to compute the detectability distance for the different models. This is the value appearing in the last column of Table 2, and it has been computed

taking into account the detailed response of INTEGRAL’s SPI (Jean 1995). We have assumed an observation lasting only 10 hours, in order to obtain good sensitivities when the flux in the continuum is still high. All the observations start 5 hours after peak temperature. All the computed models, except the low-mass CO nova (B1), could be detected in the continuum up to the Galactic center.

## 4.2 Lines

Lines are the best candidates for the detection of novae. This is particularly true in the case of a high resolution spectrometer like INTEGRAL’s SPI because a flux emitted in a narrow line is detected with these instruments with significances much higher than if it was spread in a broad band. The strongest  $\gamma$ -ray lines emitted by CO and ONe novae are shown in figures 1 to 4, where the spectral evolution of models A1, A2, B1 and B2 during the first 2 days is displayed. Two phases can be distinguished in the evolution of all lines. During the early nova expansion (up to a week, depending on the model), the envelope is optically thick and the intensity is not only determined by the instantaneous abundance of the parent isotopes but also by their distribution as a function of the optical depth (which depends on densities and expansion velocities). At this stage, the evolution of lines is affected by two timescales: the decay times of the radioactive isotopes and the characteristic timescale of envelope expansion. This phase includes both the rise of the intensity of the long-lived 1275 keV and 478 keV lines, and the rise and decay of the 511 keV line. Later on, when the effects of absorption and comptonization become negligible, the intensity of the lines is determined by the total mass of the radioactive isotopes and the evolutionary timescale of the 1275 keV and the 478 keV lines simply corresponds to the decay times of  $^{22}\text{Na}$  and  $^7\text{Be}$  (see figures 6 and 7, where light curves for the 1275 and 478 keV lines are shown for ONe and CO novae, respectively). However, even at late times line profiles (which have to be taken into account to determine the detectability of the lines) are determined by the distribution of  $^{22}\text{Na}$  and  $^7\text{Be}$ .

### 4.2.1 The 478 keV and 1275 keV lines

The observation of any of these lines would allow to discriminate between ONe (A1 and A2) and CO novae (B1 and B2). While the 1275 keV line can only be observed in the case of ONe novae (a negligible  $^{22}\text{Na}$  amount is produced by CO novae), the reverse is true for the 478 keV line, except for model A2, where a small amount of  $^7\text{Be}$  (see Table 1) leads to a weak line at 478 keV (see figures 1 to 4). In Table 3, we summarize the epoch of the maximum, the total line flux at maximum and the detection distances for the lines at  $3\sigma$  significance. These detection distances have been computed for INTEGRAL’s SPI assuming an observation time of  $10^6$  s starting at maximum. In all cases, the detection distances are  $\sim 0.5$  kpc. For the computation of the detection distances, we have taken into account the profiles of the lines: typical widths (FWHM) when the envelope is transparent are in the range between 3 keV (model B1) and 7 keV (model B2), for the 478 keV line, and around 20 keV for the 1275 keV one (for both A1 and A2 models).

**Table 2.** Positions and intensities of the flux maxima in the continuum (170 keV–470 keV) for the different models. Subscript 1 corresponds to values (if they exist) for the maxima associated with  $^{13}\text{N}$  decay, while subscript 2 corresponds to maxima associated with  $^{18}\text{F}$  decay. At  $t_{\text{off}}$ , the flux in the continuum falls below  $10^{-6}$  photons/s/cm $^2$ . D is the maximum detectability distance for INTEGRAL’s SPI (see text).

Model	$t_1$ [hours]	Flux $_1$ [photons/s/cm $^2$ ]	$t_2$ [hours]	Flux $_2$ [photons/s/cm $^2$ ]	$t_{\text{off}}$ [days]	D [kpc]
A1	-	-	5.5	$7.4 \cdot 10^{-2}$	7.5	8.8
A2	-	-	5	$9.1 \cdot 10^{-2}$	7.5	8.8
B1	1	$1.7 \cdot 10^{-3}$	8.4	$8.3 \cdot 10^{-4}$	1.4	1.1
B2	1	$1.7 \cdot 10^{-1}$	6.2	$5.7 \cdot 10^{-2}$	1.7	8

The rise phase for the 1275 keV line lasts  $\sim 7$  days. Soon after the maximum, the light curve reaches the stable decline phase with the expected decay time of 3.75 years. During this phase, the line intensities are directly determined from the ejected  $^{22}\text{Na}$  mass of each model, which grows with the mass of the progenitor white dwarf (Table 1), a tendency that had been previously pointed out by other authors (Starrfield et al. 1993, Politano et al. 1995).

On the basis of the calculations by Starrfield et al. (1978), Clayton (1981) first suggested that the 478 keV line produced by the decay of  $^7\text{Be}$  could be detectable for a nearby nova. This possibility was subsequently discarded by the results obtained by Boffin et al. (1993), who considered an updated reaction network, but did one-zone model nucleosynthesis calculations. The new calculations performed by Hernanz et al. (1996) show that convection plays an important role and that an appreciable amount of  $^7\text{Be}$  is produced by a CO nova. The possible detection of the corresponding 478 keV line would be an important confirmation of the thermonuclear runaway model for novae and its associated nucleosynthesis. In fig. 7 we distinguish two phases in the evolution of the 478 keV line for the two CO models. During the first  $\sim 1.5$  days after peak temperature, the intensity of the line is completely dominated by the contribution of the very strong continuum generated by  $^{13}\text{N}$  and  $^{18}\text{F}$  emission. During this epoch, the line reaches its absolute maximum. Later on, the contribution of the continuum disappears and the line follows a “typical” light curve. The properties of the line at its late maximum are shown in Table 3. This late maximum is reached at day 5 for the massive CO nova B2 ( $F=2.6 \cdot 10^{-6}$  photons/s/cm $^2$ ). The low-mass CO nova, B1, has a less intense maximum ( $F=1.4 \cdot 10^{-6}$  photons/s/cm $^2$ ), related to its lower  $^7\text{Be}$  content, appearing later ( $t \sim 13$  days), because it is more opaque.

#### 4.2.2 The 511 keV line

This line is expected to be, by far, the strongest  $\gamma$ -ray feature emitted by any nova and it appears with high intensity in all models. However, it is much fainter in the low-mass CO model (B1), which has a more opaque envelope because of its higher mass and lower velocity. Several isotopes contribute to the 511 keV emission (see section 1), with decay times ranging from minutes to years. This results in a relatively complex temporal evolution. Besides, as the line reaches its maximum during the 10 first hours after peak temperature, when the envelope is optically thick, its intensity is strongly affected by the details of the distribution of the radioactive nuclei and the expansion velocities. Thus its detection would provide critical information about the properties of novae

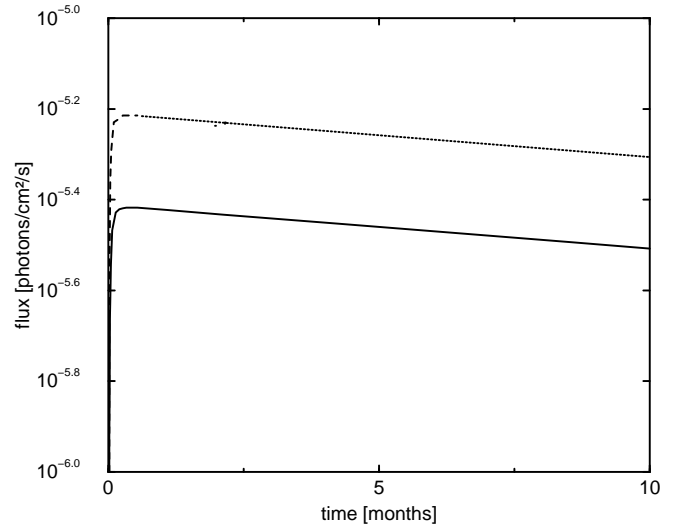


**Figure 6.** Light curves for the 1275 keV line ( $d=1$  kpc). Solid line corresponds to model A1 ( $1.15 M_{\odot}$ , ONe nova) and dashed line corresponds to A2 ( $1.25 M_{\odot}$ , ONe).

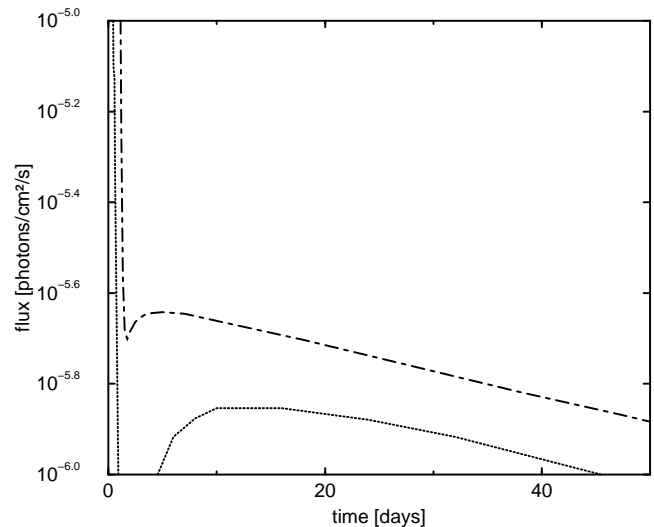


**Figure 7.** Light curves for the 478 keV line ( $d=1$  kpc). Dotted line corresponds to model B1 ( $0.8 M_{\odot}$ , CO nova), whereas dot-dashed line corresponds to model B2 ( $1.15 M_{\odot}$ , CO).

**Table 3.** Properties of the 478 keV and 1275 keV lines: time and flux at maximum for an assumed distance of 1 kpc. D is the maximum detectability distance for INTEGRAL’s SPI (see text).

Model	line	t [days]	Flux [photons/s/cm <sup>2</sup> ]	D [kpc]
A1	1275 keV	7.5	3.8 10 <sup>-6</sup>	0.5
A2	1275 keV	6.5	6.1 10 <sup>-6</sup>	0.6
B1	478 keV	13	1.4 10 <sup>-6</sup>	0.4
B2	478 keV	5	2.6 10 <sup>-6</sup>	0.5

**Table 4.** Properties of 511 keV line: time and flux at maximum for an assumed distance of 1 kpc. D is the maximum detectability distance for INTEGRAL’s SPI (see text).

Model	t [hours]	Flux [photons/s/cm <sup>2</sup> ]	D [kpc]
A1	6	1.3 10 <sup>-2</sup>	13.5
A2	5	1.6 10 <sup>-2</sup>	12.5
B1	1/7.5	1.7 10 <sup>-3</sup> /1.4 10 <sup>-4</sup>	1.6
B2	1/6.5	10 <sup>-2</sup> /7.3 10 <sup>-3</sup>	9

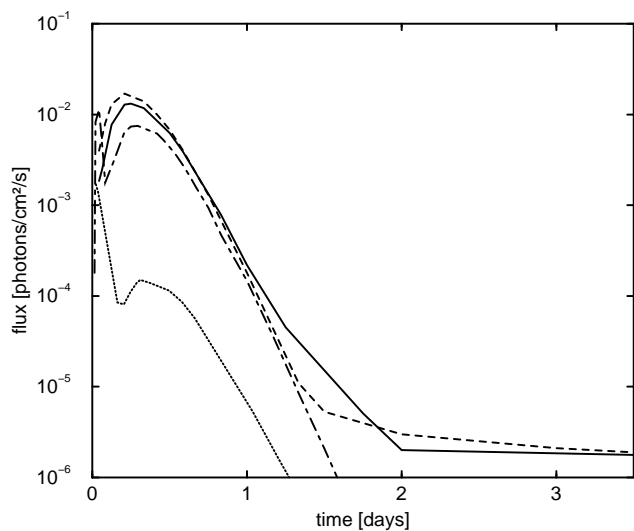


**Figure 8.** Light curve evolution for the 511 keV line ( $d=1$  kpc). Solid line corresponds to model A1 (1.15  $M_{\odot}$ , ONe nova), dashed line to model A2 (1.25  $M_{\odot}$ , ONe), dotted line to model B1 (0.8  $M_{\odot}$ , CO) and dot-dashed line to model B2 (1.15  $M_{\odot}$ , CO).

ejecta. The properties of the line in the different models appear in Table 4, whereas the light curves are displayed in figure 8. As happens with the continuum, the 511 keV line shows two maxima in models B1 and B2, which are related to the decay of  $^{13}\text{N}$  and  $^{18}\text{F}$ , while the first maximum does not appear in models A1 and A2. The maximum intensities are shown in Table 4. Light curves for models A1 and A2 are very similar, specially in the period between 0.5 days and 1 day after peak temperature. The intensity of the late maximum for model B2 is approximately 2 times smaller than that of models A1 and A2, although later than 12 hours after peak temperature its light curve converges with those of models A1 and A2. Model B1 emits lower fluxes at the two maxima (around 100 times smaller than ONe models for the second maximum), because of the larger optical thickness at these early epochs. Later than 2 days after peak temperature, models A1 and A2 present a more stable emission at 511 keV produced by the contribution of  $^{22}\text{Na}$  which emits a  $e^+$  in 90 % of its decays. As happens for the continuum

(see above), this remaining emission totally disappears later than a week after peak temperature, when positrons emitted by  $^{22}\text{Na}$  freely escape without annihilating.

For the estimation of the maximum distances for detectability (see Table 4), we have adopted in this case the same observation parameters as for the continuum, because of the shortness of the 511 keV emission (for comparison, the sensitivity offered by OSSE, on board CGRO satellite, at 511 keV is approximately 10 times worse than that offered by INTEGRAL’s SPI for the same conditions). For models A1, A2 and B2, the line would be observed at distances equivalent to the Galactic center (13.5 kpc, 12.5 kpc and 9 kpc) although the Galactic center itself should be avoided because of its 511 keV characteristic emission. The lower intensity of the 511 keV line for the low-mass CO nova, B1, makes it only detectable for a distance smaller than 1.6 kpc. The typical width (FWHM) of the 511 keV line is 8 keV (except for model B1, which has a width of 3 keV).

The fundamental difficulty posed by the detection of the 511 keV line is, of course, its short duration. The detectability of the line critically depends on the time at which the observation starts. To visualize this dependence, we have computed the maximum distance of detection for a 10 hours observation as a function of the starting time of the observation (Fig. 9). It is easy to appreciate from the figure how fast the chances of detection decline. The maximum distance of detection falls below 1 kpc if the observation starts later than  $\sim 20$  hours after peak temperature. Thus a strategy for early detection of novae is necessary in order to observe this emission. A chance is offered by the fact that INTEGRAL will spend an important part of its observation time performing a survey of the Galactic plane, where most of the novae are expected to occur. Because of its large field of view ( $\sim 16^\circ$ ), the possibility of an early nova detection by INTEGRAL’s SPI during the survey is not negligible.

## 5 DISCUSSION AND CONCLUSIONS

It is important to mention that all theoretical models, including ours, do not fit some of the ejected masses observed in novae eruptions (although not all observations of the same nova give the same value of the ejected mass). As an example, our ONe model A1 ( $M_{\text{wd}}=1.15$ ) fits quite well the observed abundances of the neon nova QU Vul 1984, but

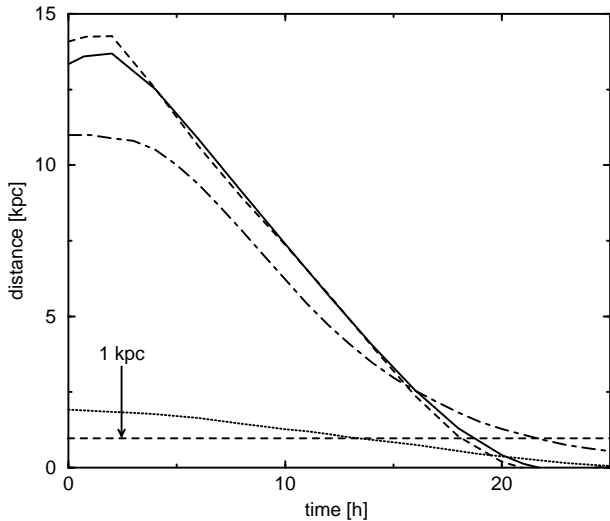


**Figure 9.** Maximum distance of detection for the 511 keV line emission as a function of the starting observation time. Solid line corresponds to model A1 ( $1.15 M_{\odot}$ , ONe nova), dashed line to model A2 ( $1.25 M_{\odot}$ , ONe), dotted line to model B1 ( $0.8 M_{\odot}$ , CO) and dot-dashed line to model B2 ( $1.15 M_{\odot}$ , CO). The results correspond to a 10 hours observation with INTEGRAL’s SPI.

the ejected mass of this nova deduced from observations is between  $2 \times 10^{-5}$  and  $\sim 10^{-3} M_{\odot}$  (Saizar et al. 1992), almost two orders of magnitude larger than the theoretical one in the most unfavourable case. Thus, the flux of the 1275 keV line could be considerable larger for some particular ONe nova, but no present theoretical models are able to produce simultaneously such large ejected masses and neon in the ejecta (see Shara 1994, Shara & Prialnik 1994 and Starrfield et al. 1997 for recent discussions and some suggestions relative to this problem). In view of this still open problem, we have made some estimations of the effect of the mass of the envelope, as well as the mean velocity of the ejecta, in the flux of the predicted  $\gamma$ -ray lines. Concerning the 511 keV line, an increase by a factor of  $\sim 20$  in the ejected mass only reduces the flux at maximum by a factor of  $\sim 3$ . On the other hand, a reduction of the speed by a factor of  $\sim 8$  reduces the flux by a factor of  $\sim 100$ . Concerning the medium and long lived-emission from  ${}^7\text{Be}$  and  ${}^{22}\text{Na}$  (at 478 and 1275 keV, respectively), ejected mass influences in the expected way the fluxes (a factor of 10 increase in mass leads to a factor 10 increase in flux), because that emission is mainly produced when the envelope is transparent. By the same reason, the velocity only influences the rise to maximum, because this is the phase where transparency plays an important role.

One of the main conclusions of our study is that the  $\gamma$ -ray signatures of CO and ONe novae are very different, except for the early emission. During the first hours after explosion (i.e. after peak temperature or roughly after peak bolometric luminosity), continuum emission below 511 keV dominates, as well as an intense line at 511 keV, for all the models. But this emission can more easily be detected “a posteriori”, with a retrospective analysis of the data from instruments like BATSE on board CGRO (Fishman et al. 1991). The reason is that this early emission happens most probably before the maximum in visual magnitude and even

before detection for the majority of novae: around 2 days before visual maximum for a very fast nova, between 2 and 5 days for a fast nova and between 5 and 10 days before maximum for a moderately fast nova; the majority of ONe novae have been classified as fast novae. We are mainly concerned by moderately fast to very fast novae, because these are the most luminous ones and thus also the most easily detectable either in visual or in  $\gamma$ -rays. Concerning the late emission, it is very different in a CO nova than in an ONe one. In the first case, emission from  ${}^7\text{Be}$  at 478 keV is obtained, with fluxes lasting for some months but just in the limit of detectability by present and future instruments (see however our comment concerning ejected masses, which applies both to CO and to ONe novae). A similar situation concerning detectability occurs in the ONe case, but related to the 1275 keV line, which lasts around 3 years. We understand why neon novae have not been detected by COMPTEL, and we are moderately optimistic concerning the future SPI instrument on board INTEGRAL, specially if a nearby and high envelope mass nova explodes during the duration of the mission.

## ACKNOWLEDGMENTS

We are specially indebted to Pierre Jean, who provided us with information about the SPI spectrometer of the future INTEGRAL satellite. We thank for partial support the CI-CYT and DGICYT Projects ESP95-0091 and PB94-0827-C02-02.

## REFERENCES

- Ambwani K., Sutherland R., 1988, *ApJ* 325, 820  
 Arnett D.W., Truran J.W., 1969, *ApJ*, 157, 339  
 Boffin H.M.J., Paulus G., Arnould M., Mowlavi N., 1993, *A&A*, 279, 173  
 Bussard R.W., Ramaty R., Drachman R.J., 1979, *ApJ*, 228, 928  
 Chan K.W., Lingenfelter R.E., 1993, *ApJ*, 405, 614  
 Clayton D.D., 1981, *ApJ*, 244, L97  
 Clayton D.D., Hoyle F., 1974, *ApJ*, 187, L101  
 Diehl R., et al., 1995, *A&A*, 298, 445  
 Fishman G.J. et al., 1991, in Durouchoux P., Prantzos N., eds., *Gamma-Ray Line Astrophysics*. AIP, New York, p. 190  
 Gómez-Gomar J., Isern J., Jean P., 1997, *MNRAS*, in press  
 Harris M.J., Leising M.D., Share, G.H., 1991, *ApJ*, 375, 216  
 Harris M.J., Purcell W.R., Grabelsky D.A., Johnson W.N., Jung G.V., Kinzer R.L., Kurfess J.D., McNaron-Brown K., Strickman M.S., Ulmer M.P., 1996, *A&AS*, 120, 343  
 Hernanz M., José J., Coc A., Isern J., 1996, *ApJ*, 465, L27  
 Hernanz M., Gómez-Gomar J., José J., Isern J., 1997a, in 2<sup>nd</sup> INTEGRAL Workshop “The transparent Universe”. ESA SP-382, Noordwijk, p. 47  
 Hernanz M., Gómez-Gomar J., José J., Isern J., 1997b, in 4<sup>th</sup> COMPTON Symposium. AIP, New York, in press  
 Iyudin A.F., Bennett K., Bloemen H., Diehl R., Hermsen W., Lichti G.G., Morris D., Ryan J., Schönfelder V., Steinle H., Strong A., Varendoff M., Winkler C., 1995, *A&A*, 300, 422  
 Jean P., 1995, private communication  
 José J., 1996, PhD. Thesis, University of Barcelona  
 José J., Hernanz M., 1997a, *ApJ*, in press (astro-ph/9709153)  
 José J., Hernanz M., 1997b, *Nucl. Phys.*, A621, 491c  
 José J., Hernanz M., Coc A., 1997, *ApJ*, 479, L55  
 Leising M.D., Clayton D., 1987, *ApJ*, 323, 159



- Leising M.D., Share G.H., Chupp E.L., Kanbach G., 1988, *ApJ*, 328, 755
- Nofar I., Shaviv G., Starrfield S., 1991, *ApJ*, 369, 440
- Ore A., Powell J.L., 1949, *Phys. Rev.*, Vol. 75, 11, 1696
- Pozdnyakov L.A., Sobol I.M., Sunyaev R.A., 1983, *Soviet Scientific Reviews. Section E: Astrophysics and Space Physics Reviews*, Vol 2, p. 184
- Politano M., Starrfield S., Truran J.W., Weiss A., Sparks W.M., 1995, *ApJ*, 448, 807
- Prantzos N., Diehl R., 1996, *Phys. Rep.*, 267, 1
- Prialnik D., Kovetz A., 1997, *ApJ*, 477, 356
- Prialnik D., Shara M., Shaviv G., 1979, *A&A*, 72, 192
- Ritossa C, García-Berro E., Iben I., 1996, *ApJ*, 460, 489
- Saizar P. et al., 1992, *ApJ*, 398, 651
- Shara M.M., 1994, *AJ*, 107, 1546
- Shara M.M., Prialnik D., 1994, *AJ*, 107, 1542
- Prialnik D., Kovetz A., 1997, *ApJ*, 477, 356
- Starrfield S., Truran J.W., Sparks W.M., Arnould M., 1978, *ApJ*, 222, 600
- Starrfield S., Truran J.W., Politano M., Sparks W.M., Nofar I., Shaviv G., 1993, *Phys. Rep.*, 227, 223
- Starrfield S., Truran J.W., Wiescher M., Sparks W.M., 1997, *MNRAS*, in press
- Weiss A., Truran J.W., 1990, *A&A*, 238, 178
- Wood P.R., 1974, *ApJ*, 190, 609